# A Closed-Loop Controlled Nanomanipulation System for Probing Nanostructures Inside Scanning Electron Microscopes

Chao Zhou, Zheng Gong, Brandon K. Chen, Zhiqiang Cao, Junzhi Yu, *Senior Member, IEEE*, Changhai Ru, Min Tan, Shaorong Xie, and Yu Sun, *Fellow, IEEE*

***Abstract*—Probing nanostructures (e.g., nanoelectronics) requires accurate and precise nanopositioning. Furthermore, since measuring *I–V* data from dc to GHz typically takes more than a minute, tolerance for position drift is stringent during the data collection process. This paper reports a closed-loop controlled nanomanipulation system for operation inside a scanning electron microscope. A new position sensing method with low power consumption is used to achieve nanometer sensing resolution and effective heat dissipation management. For automated probing of nanostructures, the position sensor-based closed-loop probing approach was found to be four times faster than visually servoed probing, and ten times faster compared to manual operation. Probing accuracy was determined to be better than 3 nm and a drift rate lower than 1 nm/min.**

***Index Terms*—Nanopositioning, nanomanipulation, probing nanostructures.**

Manuscript received May 8, 2015; accepted February 6, 2016. Date of publication February 23, 2016; date of current version April 28, 2016. Recommended by Technical Editor G. Cherubini. This work was supported in part by the Natural Sciences and Engineering Research Council of Canada, Ontario Ministry of Research and Innovation (ORF-RE funding), and Hitachi High-Technologies Canada Inc., in part by the National Natural Science Foundation of China (61473295, 61528304, 71401189, and 51575333), in part by Beijing Natural Science Foundation (4152054), the International S&T Cooperation Program of China (2014DFA70470), the Instrument Development Major Program of National Natural Science of China (61327811), and the Shanghai Municipal Science and Technology Commission Project (14JC1491500).

C. Zhou, Z. Cao, J. Yu, and M. Tan are with the State Key Laboratory of Management and Control for Complex Systems, Institute of Automation, Chinese Academy of Sciences, Beijing 100190, China (e-mail: chao.zhou@ia.ac.cn; zhiqiang.cao@ia.ac.cn; junzhi.yu@ia.ac.cn; min.tan@ia.ac.cn).

Z. Gong, B. K. Chen, and Y. Sun are with the Advanced Micro and Nanosystems Laboratory, University of Toronto, Toronto, ON M5S 3G8, Canada (e-mail: zgong@mie.utoronto.ca; brandon.chen@utoronto.ca; sun@mie.utoronto.ca).

C. Ru is with the Jiangsu Provincial Key Laboratory of Advanced Robotics & Collaborative Innovation Center of Suzhou Nano Science and Technology, Soochow University, Suzhou 215000, China (e-mail: rzh@suda.edu.cn).

S. Xie is with the Department of Mechatronic Engineering, Shanghai University, Shanghai 200072, China (e-mail: srxie@shu.edu.cn).

This paper has supplementary downloadable material available at http://ieeexplore.ieee.org provided by the authors. Two demos are included in this video. The first is automated nanoprobing of four predefined positions over a span of 35 minutes for 360 cycles. The second one is automated nanoprobing of duplicated features. This material is 18.1 MB. Contact sun@mie.utoronto.ca for further questions about this work.

Color versions of one or more of the figures in this paper are available online at http://ieeexplore.ieee.org.

Digital Object Identifier 10.1109/TMECH.2016.2533636

## I. Introduction

As the integrated circuits (IC) industry continues its miniaturization trend, nanometer-sized nanoelectronic structures need to be probed for design verification and manufacturing quality monitoring. Nanoelectronic probing is often performed inside a scanning electron microscope (SEM) with piezoelectric nanomanipulators. Real-time SEM image feedback and precise positioning of probes via a nanomanipulation system offer significant speed advantages over atomic force microscopy-based probing. State-of-the-art SEM-based nanoprobing is conducted by highly trained personnel via joystick tele-operation, a process that is time consuming, is highly skill dependent, and has poor repeatability. To alleviate these challenges and achieve automated nanoprobing, a closed-loop controlled system is needed.

Several nanomanipulation systems have been reported in the literature [1]–[5]. There are also commercially available nanomanipulation systems developed by Kleindiek, DCG Systems (Previously Zyvex), SmarAct, Klocke, and Attocube. These systems have been applied to nanomaterial characterization [6]–[12], micro-nano device assembly [13], [14], photonics [15], [16], and biology research [17]–[19]. We previously also reported an SEM load-lock-compatible nanomanipulation system [20] driven by piezomotors and piezoactuators to selectively remove silicon nanowires for the construction of field-effect transistor nanowire protein sensors with well-controlled nanowire number and diameter bridging the source and drain electrodes [14].

Utilizing SEM image feedback, several automated operations have been demonstrated, including the handling of micro-nanomaterials [21]–[25], micro-nano device assembly [14], nanomaterial characterization [26], [27], and nanoprobing [28], [29]. These automation techniques are limited by the low imaging frame rate of SEM ($\sim$15 Hz) and are susceptible to SEM imaging conditions (e.g., brightness fluctuation, image drift, and image noise).

Automation can also be realized via the integration of position sensors for closed-loop positioning. Optical encoder-based sensors generate heat that is difficult to dissipate inside SEM's high vacuum environment, causing nearby materials to thermally expand and result in drift. Capacitive sensors are costly and intricate to integrate into nanomanipulation systems due to the demand for carefully routing sensing signals over long distances (e.g., 10 cm) between nanomanipulators and the feedthrough

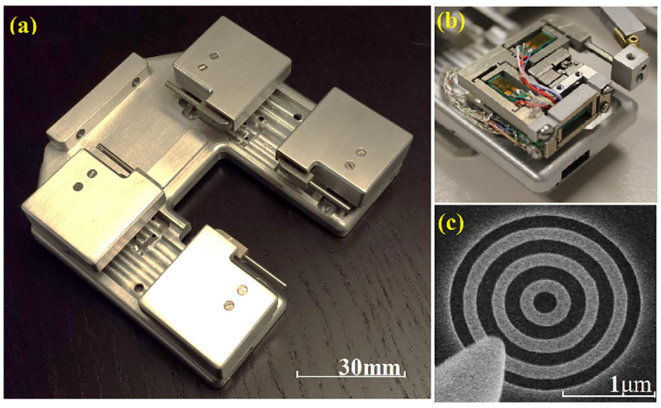


Fig. 1. (a) Nanomanipulation system with closed-loop controlled fine positioners. (b) Flexure guided, preloaded piezo fine positioner with a single strain gauge integrated. (c) Example nanoprobing targets.

flanges on an SEM. Strain gauge-based sensing is sensitive to temperature change, and the traditional sensing circuitry with the Wheatstone bridge configuration and signal amplifiers generates significant heat that leads to sensing signal drift.

This paper reports a new nanomanipulation system with a position sensing method based on strain gauges and time-to-digital conversion (TDC). This method requires low power because the measurement method is based on the charging of a capacitor. The system consists of long range coarse positioners and high precision fine positioners. Closed-loop nanoprobing was demonstrated and quantitatively evaluated. The experimental results demonstrate that the system is capable of performing automated probing of nanostructures under IC-chip-probing relevant electron microscopy imaging conditions. The nanomanipulation system has sub-nanometer sensing resolution, a sensing signal drift rate that is lower than 1 nm/min, and a closed-loop positioning accuracy better than 3 nm.

Our previous publications [28], [29] described the use of real-time SEM image denoising and drift compensation to enable automated probing. The main limitation of the approach is the slow frame rate of SEM (15 Hz). The approach reported in this paper utilizes strain gauge sensory feedback with 100 Hz bandwidth, allowing higher speed automated probing. In addition, the automation shown in this paper is no longer susceptible to the random SEM image fluctuations due to external magnetic field and thermal image drift. The automated probing can be performed even when the SEM electron beam is turned off, which minimizes electron beam damage to the sample.

In this paper, system design is introduced in Section II. Section III presents characterization details of the position sensors and the control system. Section IV describes nanoprobing experiments and performance evaluation of the system for automated probing of nanostructures. Finally, Section V concludes this paper.

## II. System Design

The nanomanipulation system (see Fig. 1) consists of four manipulators centrally mounted on a load-lock compatible carrier. The system can be transferred in and out of SEM through the vacuum load-lock, eliminating the need to break the high vacuum within the SEM chamber during sample and end-tool changes.

To enable closed-loop controlled nanoprobing, position feedback is required to be repeatable, accurate, and with minimal drift. In this work, the nanomanipulation system integrates a new position sensing method. It is critical to design the position sensing electronics with minimized heat generation, allowing the overall system to efficiently reach thermal equilibrium quickly. By maintaining thermal equilibrium, thermal expansion or contraction of the system structural elements is reduced, and the sensing elements that are sensitive to temperature changes are not significantly affected.

### A. Manipulators

Each manipulator consists of three long range coarse positioners with three high precision fine positioners stacked on top. The coarse positioners are composed of three stick-slip-based piezo positioners for *XYZ* coarse positioning. In this design, no sensory feedback is implemented in the coarse positioners to minimize heat generation sources. Stainless steel rail construction improves guiding accuracy and ensures efficient heat dissipation. Coarse positioning is open-loop controlled and only needs to move end effectors (e.g., tungsten probes) into the field of view of SEM.

The fine positioners are three flexure guided, preloaded piezo positioners with one strain gauge mounted on each piezostack. Unlike the use of traditional Wheatstone bridge configuration that requires up to four strain gauges mounted on a single piezo to maximize sensitivity, our single strain gauge method provides comparable sensitivity while using significantly less power. Using position feedback, the system is able to control the fine positioners via closed-loop control to probe nanoscaled structures. In the automated mode, end effectors are moved by the system to reach specified target coordinates with a high repeatability and accuracy. After the coarse positioners bring the end-effector into the field of view, if this distance between a target and the end-effector is larger than the remained motion range of fine positioners, position sensing signals stay constant before the end-effector reaches the target although actuation voltages are increased. This prompts the actuation of the coarse positioners again and readjustment of the fine positioners.

### B. Sensor Design

Strain gauges and the Wheatstone bridge for sensing strain in piezostacks are commonly used in the air environment where four strain gauges are glued to the surfaces of a piezostack to form a full-bridge circuit configuration for maximizing sensitivity. When the piezostack expands or contracts, strain-induced resistance changes in the strain gauges are converted to voltage changes by the Wheatstone bridge. The method requires a relatively large piece of piezostack to accommodate four strain gauges, which increases the overall size of fine positioners. In the vacuum environment, heat generated from the four strain gauges is mainly conducted through the ceramic piezostack that has poor thermal conductivity. Inefficient heat transfer in vacuum

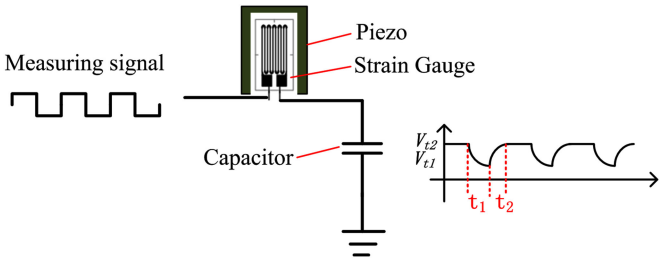


Fig. 2. Charging and discharging of a capacitor through a strain gauge.

causes thermal expansion in both the strain gauges and the piezostack, resulting in sensor and actuator drift. Additionally, circuitries for amplifying Wheatstone bridge readout also generate heat that is difficult to dissipate in the vacuum environment.

In this paper, we developed a strain gauge sensing method that is more suitable for use in vacuum. As shown in Fig. 2, a single strain gauge is mounted on a piece of piezostack and connected in series with a capacitor. When no strain is applied to the strain gauge, the resistance of the strain gauge remains constant, and the time it takes to charge and discharge the capacitor remains constant. When the resistance of the strain gauge changes due to applied strain, the time it takes to charge and discharge the capacitor changes, thus can be correlated to strain changes [30].

The charging and discharging time can be accurately measured using a TDC, and correlated to resistance change in strain gauge according to (1). It is feasible to obtain high accuracy time measurement with TDC, which leads to a more accurate strain measurement than the Wheatstone bridge

$$\begin{aligned} t_1 &= R \cdot C \cdot \ln\left(\frac{V_{t2}}{V_{t1}}\right) \\ t_2 &= R \cdot C \cdot \ln\left(\frac{V_{\rm cc} - V_{t1}}{V_{\rm cc} - V_{t2}}\right) \end{aligned} \tag{1}$$

where $V_{\rm cc}$ is the voltage of a fully charged capacitor; $V_{t1}$ and $V_{t1}$ are the threshold voltage of charging; and $t_1$ and $t_2$ are the discharging and charging time, respectively.

The proposed strain gauge sensing method uses approximately 200 times less power than the conventional Wheatstone bridge configuration, and approximately 50 times less power than optical encoders with comparable sensing performance. The low heat generation feature allows the overall nanomanipulation system to quickly reach thermal equilibrium and effectively maintain it. The surface area on a piezostack needed for mounting strain gauge is also reduced by four times, allowing smaller fine positioners to be constructed.

The TDC circuit built in this work is based on the measurement of charging and discharging time of a capacitor through the strain gauge. The circuit has a higher complexity than the conventional Wheatstone bridge circuitry, and is presently limited to 100 Hz in bandwidth. The process of charging and discharging is typically slower than AD conversion in the conventional Wheatstone bridge. This bandwidth was intentionally designed for improving the position sensing resolution while satisfying the need of nanomanipulation inside SEM.

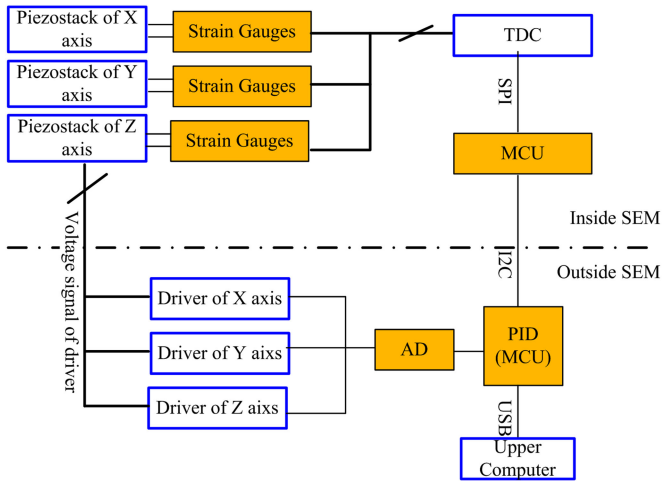


Fig. 3. Closed-loop controlled nanomanipulation system architecture. The devices of low power consumption are inside the SEM, while the ones of high power consumption are all outside.

On-board electronics is placed within the aluminum housing of the nanomanipulation system carrier inside the SEM. The strain level of the strain gauge mounted on the piezostack is measured with TDC circuitry positioned in close proximity to ensure signal integrity. Sensor output from every manipulator is collected by the on-board MCU (microcontroller unit), synchronized, filtered, and sent to the external electronics (outside SEM) via the I2C bus. Our approach minimizes sensor signal interference by reducing the length of signal wires, and allows large amount of sensor data to be transferred out of the SEM without the need for additional vacuum feedthrough wiring.

The external electronics consists of an MCU and arrays of operational amplifiers for driving the piezo stack. After receiving sensor readout from the on-board electronics, the MCU computes the required piezo stack driving voltages based on the PID control law, and sends driving voltages to the on-board electronics, as illustrated in Fig. 3.

### C. Control System

The imaging magnification of an SEM can typically be varied up to a million times. When the SEM magnification is changed, it is desired for the positioning speed and resolution of the nanomanipulation system to automatically change accordingly. Therefore, using a single set of PID controller parameter for all imaging magnifications is inadequate. Online switching of PID parameters can result in sudden changes in positioner output, which in practice may cause the delicate nanoprobe tips to collide with the sample and cause tip or sample damage. To overcome this problem, the system changes control gains gradually, and new integral term is calculated according to

$$\begin{aligned} u_t = {} & [K_{P1}S_t + K_{P2}(1 - S_t)]e_t + K_{I1}\sum_{0}^{\rm to} e_t + K_{I2}\sum_{\rm to+1}^{t} e_t \\ & + [K_{D1}S_t + K_{D2}(1 - S_t)](e_t - e_{t-1}) \end{aligned} \tag{2}$$

where $\{K_{P1}, K_{I1}, K_{D1}\}$ and $\{K_{P2}, K_{I2}, K_{D2}\}$ are the control gains to be switched; $e_t$ is the error at time $t$; and $u_t$ is the output.

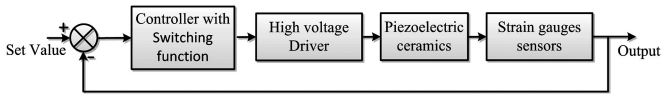


Fig. 4. Architecture of the control system.

$S_t$ is a smooth curve that is defined as

$$S_t = \begin{cases} 1 & t < t_0 \\ 1 + t_0/t_w - t/t_w & t_0 \le t \le t_w \\ 0 & t > t_w \end{cases} \quad (3)$$

where $t_o$ is the time of switching, and $t_w$ is the length of switch window.

Fig. 4 shows the control system architecture, where the deformation of piezoelectric ceramics is measured by the strain gauge sensors. A sudden change in controller parameters can cause a sudden change in controller's output (e.g., positioner making large, sudden movements). By changing controller parameters in gradual increments, we minimized the changes in controller's output. The change of proportional parameter and differential parameter is given by $S_t$ (3). This switching strategy was proven experimentally to ensure smooth controller output.

### D. Alignment of Manipulator Axes

Due to inaccuracies in machining and assembly of the nanomanipulation system components, it is infeasible to mechanically align the motion axes of each manipulator to be perfectly orthogonal to each other. Since the system contains multiple manipulators, each manipulator has its own set of coordinate system; proper alignment is important to achieve in order to avoid confusion to operators.

Using rotation matrices can compensate for the misalignments in motion axes. However, manual calibration of each motion axis under SEM is time consuming. The long calibration time results in prolonged electron beam exposure, which can cause contaminations to end-effectors and the sample due to electron beam-induced deposition [31]. Furthermore, to change an end-effector (e.g., nanoprobe) or sample, the operator needs to physically contact the nanomanipulation system, which can cause slight alterations in frictions at interfaces and create slight mechanical misalignments, demanding system recalibration.

In our system, the motion path of each manipulator axis was characterized using SEM visual feedback and corrected through online coordinate transformation to match each manipulator's axis with the SEM image axis. The transformation from positioners' reference frame to that of SEM imaging frame is

$$\begin{bmatrix} x \\ y \\ z \end{bmatrix}_{\text{SEM}} = \begin{bmatrix} \cos\alpha & -\sin\beta & \frac{d_x}{d_z} \\ \sin\alpha & \cos\beta & \frac{d_y}{d_z} \\ 0 & 0 & 1 \end{bmatrix} \begin{bmatrix} x \\ y \\ z \end{bmatrix}_{\text{pos}} \triangleq A \begin{bmatrix} x \\ y \\ z \end{bmatrix}_{\text{pos}}. \quad (4)$$

The angle between the manipulator axis and SEM image axis is $\alpha$ for the $X$-axis and $\beta$ for the $Y$-axis. Manipulator's $Z$-axis movement $d_z$ is projected onto the SEM screen as $X$–$Y$ movement due to misalignment, measured to be $d_x$ and $d_y$. In experiments, the automated calibration process takes approximately 2 min to align one manipulator. The system repeats auto calibration under each SEM imaging magnification to improve positioning accuracy when imaging magnification is changed during nanomanipulation.

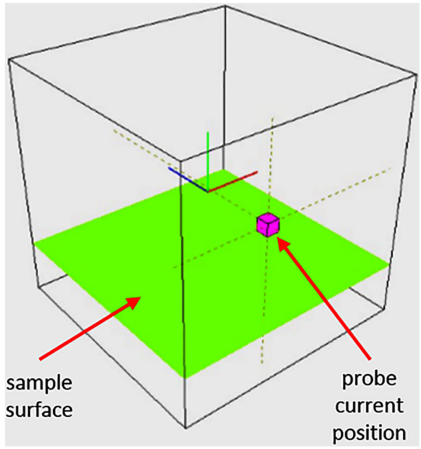


Fig. 5. Real-time graphical representation of the sample-probe location, enabled by closed-loop feedback of the system.

### E. Manipulator-Sample Registration

Nanoprobing involves landing nanometer-sized probe tips on top of IC nanostructures to establish electrical connections. Due to the lack of depth information from 2-D SEM image feedback, detecting the probe-sample contact relies on operator skills. The contact detection process is time consuming, and results in probe tip or sample damage due to collision.

Because of the closed-loop capability of our nanomanipulation system, the need for manually establishing probe-sample contact every time is eliminated. The operation of our system involves manual establishment of probe-sample contact on three or more locations on the sample, and the *XYZ* coordinates are recorded. These coordinates are used by the system to determine sample position and orientation relative to the manipulators, and the result is graphically presented in the system's graphical user interface as shown in Fig. 5. From this point onwards, the system is capable of automatically establishing probe-sample physical contact using position feedback.

## III. System Characterization Results

System positioning performance was characterized in a Hitachi S4800 field emission SEM. Denoising and image stabilization algorithms [28] are employed by the system to compensate for the high image noise and image drift at high SEM imaging magnifications. SEM imaging conditions were tuned to maximize image quality at the 800000 × magnification. Characterization of the position sensor and manipulator performance was conducted using sub-pixel visual tracking [20]. Table I summarizes the overall system performance.

### A. Sensor Characterization

Sensor characterization includes the quantification of drift, linearity, resolution, and accuracy. Drift in sensor readout is mainly caused by temperature change of the strain gauges.

TABLE I
SYSTEM SPECIFICATION AND PERFORMANCE

| | | |
|---|---|---|
| Dimension | Complete system | $100 \times 100 \times 20$ mm$^3$ |
| | One manipulator | $30 \times 30 \times 17$ mm$^3$ |
| Position sensor | Resolution | $<1$ nm |
| | Accuracy | 3 nm |
| | Drift | $<1$ nm/min |
| Coarse positioner (open loop) | Range | 10 mm in $XY$, 5 mm in $Z$ |
| | Minimum step size | 112.5 nm |
| Fine positioner (open loop) | Range | $\sim 22$ $\mu$m |
| | Minimum step size | 0.12 nm |
| Fine positioner (closed loop) | Range | 20 $\mu$m |
| | Accuracy | 5 nm |
| | Maximum speed | 45 $\mu$m/s |

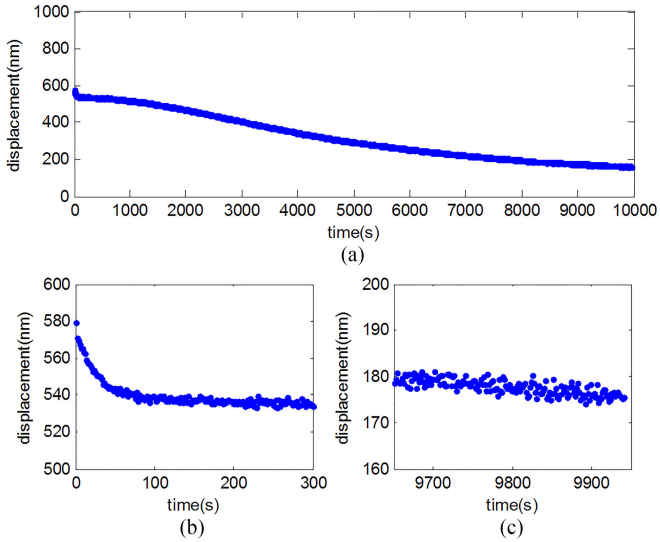


Fig. 6. Sensor drift behavior over time. (a) For the entire 10 000 s. (b) In the first 60 s of start-up, sensor readout changes drastically ($\sim$50 nm/min) due to heating of the circuit components. (c) In the last 60 s of the testing, drift has reduced to less than 0.8 nm/min.

When first placed inside the SEM, it takes some time for the nanomanipulation system to reach thermal equilibrium for optimal performance, which is applicable to any foreign object/sample placed into an SEM's vacuum chamber for thermal stability. Almost all position sensors are sensitive to temperature change due to inherent expansion/contraction in materials. The advantage of our sensing method is reduced heat generation, allowing thermal equilibrium to be quickly reached.

To study the drift behavior of our sensors within the vacuum environment, the nanomanipulation system was installed into the SEM for a few hours prior to the experiment to ensure that the system had reached thermal equilibrium within the SEM. Hence, any drift observed from the experiment was caused solely by the heating of the system's on-board electronics.

After the system was powered on without driving the piezo elements, the output of the sensors was recorded for 10 000 s, as shown in Fig. 6(a). In the first 60 s [see Fig. 6(b)], Ohmic heating of the circuitries from the on-board electronics caused a significant drift in sensor signal (approximately 50 nm/min). Due to the low power consumed by the on-board electronics, thermal equilibrium was quickly reestablished, reducing the sensor drift

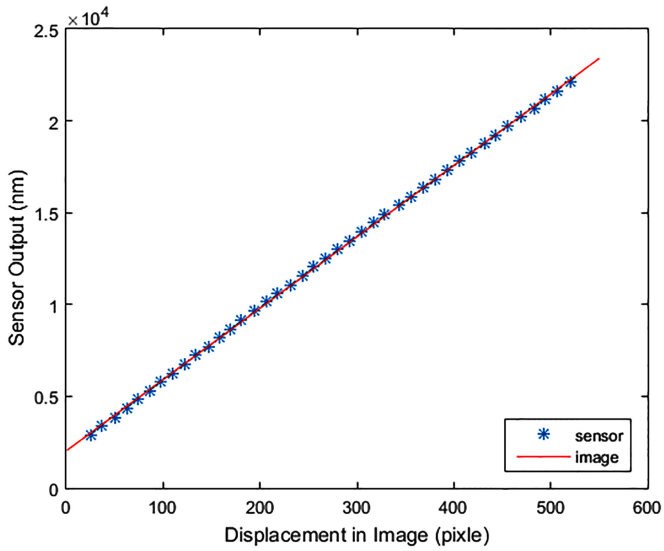


Fig. 7. Linearity of the sensor based on TDC strain gauge sensing. Each pixel at this magnification corresponds to about 37.5 nm.

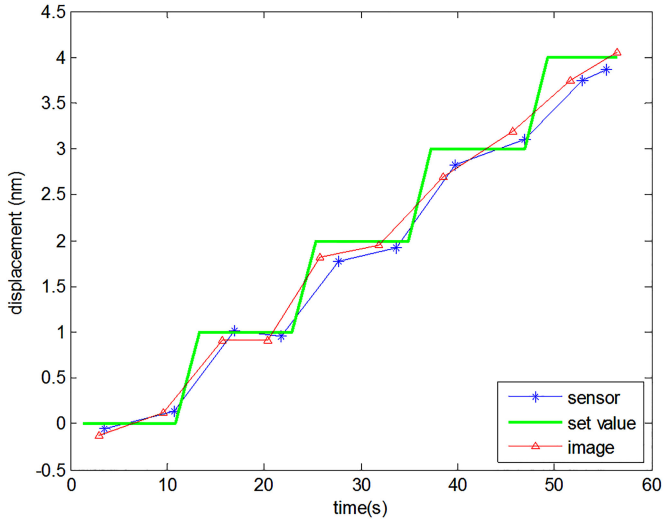


Fig. 8. Resolution of the sensor was determined to be better than 1 nm.

to less than 3 nm/min after the system was turned on for 1 min. In the last 60 s of the experiment, the sensor drift rate decreased to less than 0.8 nm/min [see Fig. 6(c)].

Compared to our previously developed system [20], which was a load-lock-compatible nanomanipulation system using optical encoder for position feedback and having a drift rate of $\sim$72 nm/min, this new sensory feedback reduced the drift rate by 90 times. During nanoprobing, it is important for the probes to stay in contact with the test points (e.g., 20–100 nm in size) without drifting away. A typical $I$–$V$ curve characterization takes less than 2 min to complete, during which our new system drifts less than 1.6 nm. This low drift rate greatly benefits reliable probing of nanoelectronics structures.

Sensor linearity represents the relationship between the system's measured input and output. In our testing, a single axis of the manipulator was operated in closed-loop mode at 80 000 magnification, taking a 2 $\mu$m motion step every 10 s over entire

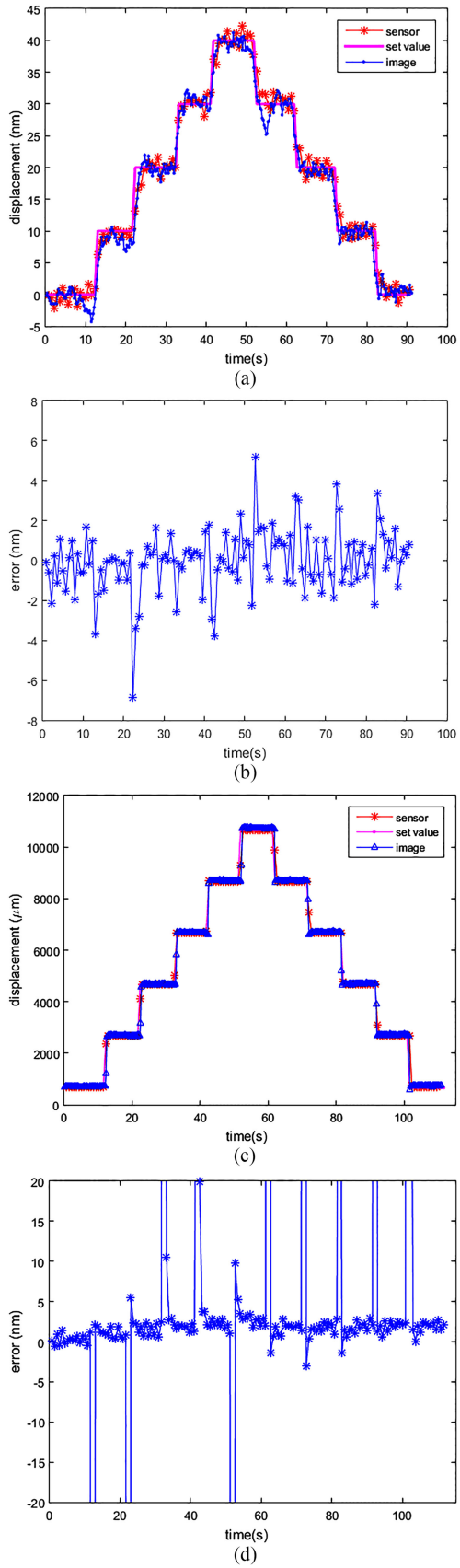


Fig. 9. Nanopositioner controller (a) 10 nm step response and (b) positioning error; (c) 2 $\mu$m step response and (d) positioning error.

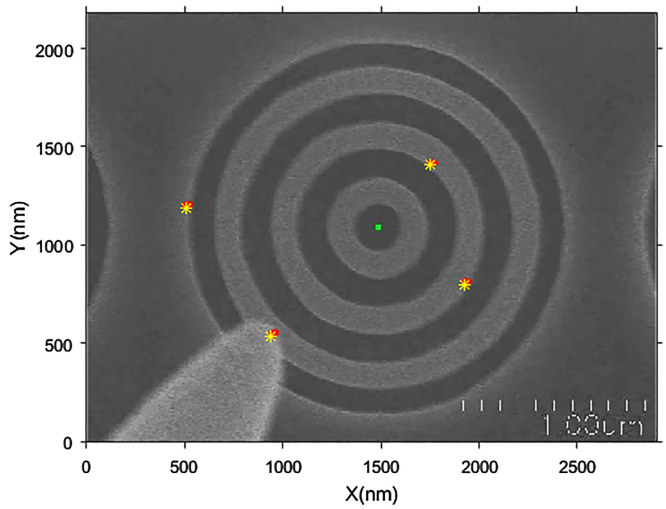


Fig. 10. Automated nanoprobing of four predefined positions over a span of 35 min. The red dots indicate the probed location in the first cycle, while the red dot shows the probed location after 360 cycles (~35 min after). Video is provided.

travel range of manipulator axis while actual positioning was visually tracked using SEM images (see Fig. 7). The r2 value of 0.9998 confirms excellent linearity of the position sensors.

To determine sensor resolution, the fine positioner was moved by 1 nm every 10 s. Fig. 8 shows a representative set of data. We read the sensors output twice after the position of end effect is changed step by step. The difference between the actual position (measured from SEM imaging) and position sensor reading is less than 1 nm, demonstrating that the position sensor has a resolution better than 1 nm.

### B. Positioning Characterization

The controller for fine positioners drives the piezo elements according to position sensory feedback. Step response and positioning error for tracking 10 nm steps and 2 $\mu$m steps are shown in Fig. 9. In Fig. 9(b), it can be seen that the difference between the image tracking result and position sensor readout overall becomes larger over time. This is because under the high SEM image magnification used (800000×), hydrocarbon contaminates were rapidly deposited within the field of view due to electron beam irradiation [31]. The deposited materials caused the feature being visually tracked to be less salient, which caused larger errors in visual tracking over time. The control performance could be improved in transient response by implementing more advanced control methods; however, in nanoprobing, manipulation is mainly taken in a small range of motion (e.g., ~100 nm), and the delay is sufficiently short for successful nanoprobing.

## IV. Nanoprobing Experiments

An SEM metrology chip from MetroBoost was used for nanoprobing tests. The chip contains arrays of identical concentric circles, each containing submicrometer lines and spacing.

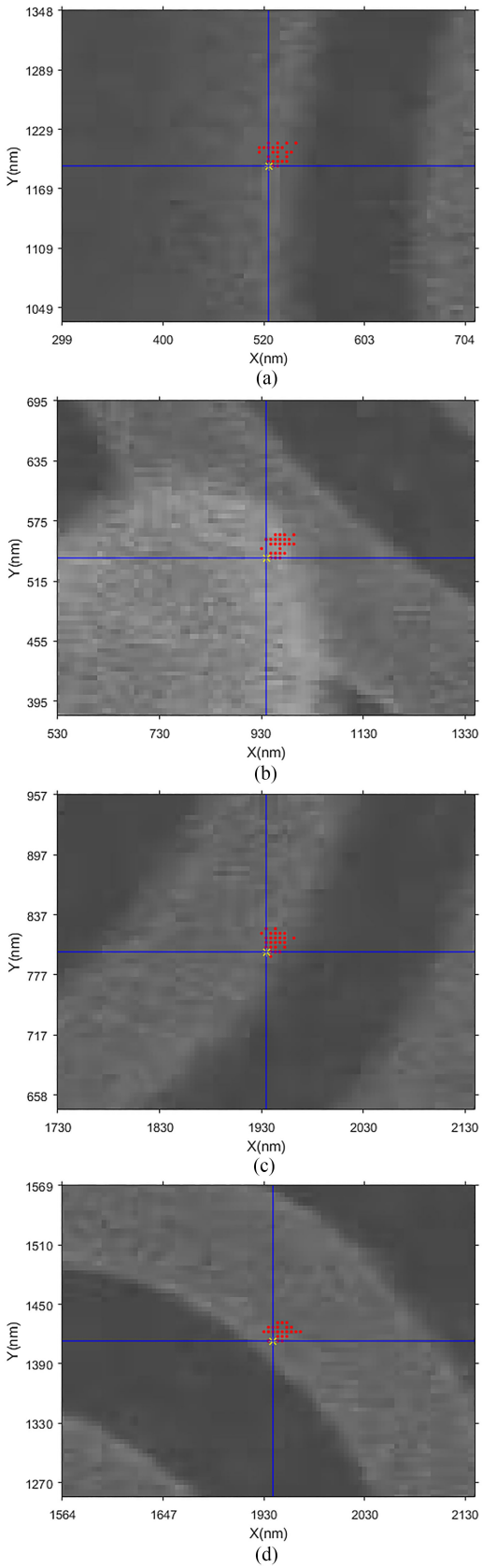


Fig. 11. Zoomed-in view of each of the probed locations. Each location is probed 360 times, and a repesentative sample of it is shown on the figure.

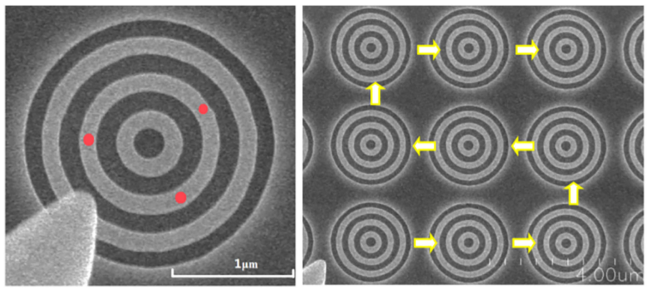


Fig. 12. Automated nanoprobing of duplicated features inside SEM.

These arrays of structures were used in this work to mimic high-density, repeated nanoelectronic components (e.g., transistors) on an IC chip (e.g., SRAM chip).

To demonstrate the long-term stability of the closed-loop nanomanipulation system, we performed a manual teaching step of probing four randomly selected locations in sequence on the concentric circle, followed by automatically performing the same probing task repeatedly and observing motion repeatability over time. During the manual teaching stage, the operator controls the motion of the manipulator with a joystick to bring the tungsten probe tip to contact with the sample, follow by saving the *XYZ* coordinate. The process is repeated four times for four randomly selected locations. During the automated probing step, the manipulator first moves in *XY*, followed by *Z* to establish probe-sample contact. The probe is then lifted by 100 nm above sample, and moved to the next saved point.

The automated probing process probed 360 locations within 35 min, and the process is shown in the first part of the Supplementary Video. Fig. 10 shows the probing results over time recorded, and Fig. 11 shows the detailed positioning history of the probe for each of the four locations. The positioning accuracy for all the four points that were each probed 360 times was $\pm 8.6$ nm. The accumulative positioning error was measured to be 35 nm at the end of the 35 min of repeated probing. In terms of probing speed, each contact took the system 1.45 s to establish. Compared to our previously reported results [28], this speed is four times faster than visually servoed nanoprobing. In addition, the nanoprobing performance does not depend upon the image quality of the SEM because of position sensor feedback, or the skill level of the human operator.

In the second half of the supplementary video, the system was operated in the learning by demonstration mode. The operator uses a joystick to probe the locations of interest on the first concentric circle. The system then performed closed-loop control to automatically probe the same locations of interest on subsequent concentric circles in the array (see Fig. 12). SEM visual feedback was used in the operator's teaching process, and the nanomanipulation system used position sensor feedback for performing subsequent automated probing without relying on SEM image feedback.

## V. Conclusion

In this paper, a closed-loop controlled nanomanipulation system that operates inside SEMs was presented. This system

integrates strain gauges for position sensing, and sensor signal was measured via the time-to-digital conversion method. Position sensor accuracy is better than 3 nm with a resolution of 1 nm. Linearity of the sensor signal throughout the 22 $\mu$m fine positioning range is higher than 0.9998. The system has a low position drift rate of 0.8 nm/min. The experimental results demonstrate that the system is capable of automated probing of nanostructures via closed-loop control via position feedback.

## References


[1] M.-F. Yu, O. Lourie, O. Lourie, K. Moloni, T. F. Kelly, and R. S. Ruoff, "Strength and breaking mechanism of multiwalled carbon nanotubes under tensile load," *Science*, vol. 287, pp. 637–640, 2000.

[2] L. Dong, F. Arai, and T. Fukuda, "Destructive constructions of nanostructures with carbon nanotubes through nanorobotic manipulation," *IEEE/ASME Trans. Mechatronics*, vol. 9, no. 2, pp. 350–357, Jun. 2004.

[3] E. C. Heeres, A. J. Katan, M. H. van Es, A. F. Beker, M. Hesselberth, D. J. van der Zalm, and T. H. Oosterkamp, "A compact multipurpose nanomanipulator for use inside a scanning electron microscope," *Rev. Sci. Instrum.*, vol. 81, pp. 023704–1–023704-4, 2010.

[4] S. Fatikow, T. Wich, H. Höulsen, T. Sievers, and M. Jöahnisch, "Microrobot system for automatic nanohandling inside a scanning electron microscope," *IEEE/ASME Trans. Mechatronics*, vol. 12, no. 3, pp. 244–252, Jun. 2007.

[5] D. Zhang, J.-M. Breguet, R. Clavel, V. Sivakov, S. Christiansen, and J. Michler, "In situ electron microscopy mechanical testing of silicon nanowires using electrostatically actuated tensile stages," *J. Microelectromech. Syst.*, vol. 19, pp. 663–674, 2010.

[6] L. X. Dong, K. Y. Shou, D. R. Frutiger, A. Subramanian, L. Zhang, B. J. Nelson, X. Y. Tao, and X. B. Zhang, "Engineering multiwalled carbon nanotubes inside a transmission electron microscope using nanorobotic manipulation," *IEEE Trans. Nanotechnol.*, vol. 7, no. 4, pp. 508–517, Jul. 2008.

[7] T. Fukuda, F. Arai, and L. Dong, "Assembly of nanodevices with carbon nanotubes through nanorobotic manipulations," *Proc. IEEE*, vol. 91, no. 11, pp. 1803–1818, Nov. 2003.

[8] D. J. Bell, L. Dong, B. J. Nelson, M. Golling, L. Zhang, and D. Gröutzmacher, "Fabrication and characterization of three-dimensional IngaAs/GaAs nanosprings," *Nano Lett.*, vol. 6, pp. 725–729, 2006.

[9] Y. Zhu, F. Xu, Q. Qin, W. Y. Fung, and W. Lu, "Mechanical properties of vapor-liquid-solid synthesized silicon nanowires," *Nano Lett.*, vol. 9, pp. 3934–3939, 2009.

[10] H. D. Espinosa, Y. Zhu, and N. Moldovan, "Design and operation of a MEMS-based material testing system for nanomechanical characterization," *J. Microelectromech. Syst.*, vol. 16, pp. 1219–1231, 2007.

[11] G. Hwang, H. Hashimoto, D. J. Bell, L. Dong, B. J. Nelson, and S. Schon, "Piezoresistive InGaAs/GaAs nanosprings with metal connectors," *Nano Lett.*, vol. 9, pp. 554–561, 2009.

[12] A. Lugstein, M. Steinmair, A. Steiger, H. Kosina, and E. Bertagnolli, "Anomalous piezoresistance effect in ultrastrained silicon nanowires," *Nano Lett.*, vol. 10, no. 8, pp. 3204–3208, 2010.

[13] H. Dai, J. Hafner, A. Rinzler, D. Colbert, and R. Smalley, "Nanotubes as nanoprobes in scanning probe microscopy," *Nature*, vol. 384, pp. 147–150, 1996.

[14] J. Li, Y. Zhang, S. To, L. You, and Y. Sun, "Effect of nanowire number, diameter, and doping density on nano-FET biosensor sensitivity," *ACS Nano*, vol. 5, pp. 6661–6668, 2011.

[15] K. Aoki, H. Miyazaki, H. Hirayama, K. Inoshita, T. Baba, K. Sakoda, N. Shinya, and Y. Aoyagi, "Microassembly of semiconductor three dimensional photonic crystals," *Nature Mater.*, vol. 2, pp. 117–121, 2003.

[16] H. Chen, C. He, C. Wang, M. Lin, D. Mitsui, M. Eguchi, T. Teranishi, and S. Gwo, "Far-field optical imaging of a linear array of coupled gold nanocubes: Direct visualization of dark plasmon propagating modes," *ACS Nano*, vol. 5, no. 10, pp. 8223–8229, 2011.

[17] M. Ahmad, M. Nakajima, M. Kojima, S. Kojima, M. Homma, and T. Fukuda, "Nanofork for single cells adhesion measurement via ESEM-nanomanipulator system," *IEEE Trans. NanoBiosci.*, vol. 11, no. 1, pp. 70–78, Mar. 2012.

[18] Z. Gong, B. K Chen, J. Liu, C. Zhou, D. Anchel, X. Li, J. Ge, D. P. Bazett-Jones, and Y. Sun, "Fluorescence and SEM correlative microscopy for nanomanipulation of sub-cellular structures," *Light Sci. Appl.*, vol. 3, art. no. e224, pp. 1–7, 2014.

[19] B. Chen, D. Anchel, Z. Gong, R. Cotton, R. Li, Y. Sun, and D. P. Bazett-Jones, "Identification of genes from nano-dissected sub-nuclear structures," *Small*, vol. 10, pp. 3267–3274, 2014.

[20] Y. L. Zhang, Y. Zhang, C. Ru, B. K. Chen, and Y. Sun, "A load-lock-compatible nanomanipulation system for scanning electron microscope," *IEEE/ASME Trans. Mechatronics*, vol. 18, no. 1, pp. 230–237, Feb. 2013.

[21] D. Jasper and S. Fatikow, "Automated high-speed nanopositioning inside scanning electron microscopes," presented at the *6th IEEE Conference on Automation Science and Engineering*, Toronto, Canada, Aug. 21–24, 2010.

[22] X. T. Ye, Y. Zhang, C. H. Ru, J. Luo, S. R. Xie, and Y. Sun, "Automated pick-place of silicon nanowires," *IEEE Trans. Autom. Sci. Eng.*, vol. 10, no. 3, pp. 554–561, Jul. 2013

[23] L. X. Dong, F. Arai, and T. Fukuda, "Electron-beam-induced deposition with carbon nanotube emitters," *Appl. Phys. Lett.*, vol. 81, pp. 1919–1921, 2002.

[24] B. K. Chen, Y. Zhang, D. D. Perovic, and Y. Sun, "MEMS microgripper with thin gripping tips," *J. Micromech. Microeng.*, vol. 21, no. 10, art. no. 105004, pp. 1–5, 2011.

[25] Y. Shen, M. Nakajima, Z. Zhang, and T. Fukuda, "Dynamic force characterization microscopy based on integrated nanorobotic AFM and SEM system for detachment process study," *IEEE-ASME Trans. Mechatronics*, vol. 20, no. 6, pp. 3009–3017, Dec. 2015.

[26] S. Zimmermann, T. Tiemerding, T. Li, W. Wang, Y. Wang, and S. Fatikow, "Automated mechanical characterization of 2-D materials using SEM based visual servoing," *Int. J. Optomechatronics*, vol. 7, pp. 283–295, 2013.

[27] J.-O. Abrahamians, B. Sauvet, J. Polesel-Maris, R. Braive, and S. Regnier, "A nanorobotic system for in situ stiffness measurements on membranes," *IEEE Trans. Robot.*, vol. 30, no. 1, pp. 119–124, Feb. 2014.

[28] Z. Gong, B. K. Chen, J. Liu, and Y. Sun, "Robotic probing of nanostructures inside scanning electron microscopy," *IEEE Trans. Robot.*, vol. 3, no. 3, pp. 758–765, Jun. 2014

[29] C. Ru, Y. Zhang, Y. Sun, Y. Zhong, X. Sun, D. Hoyle, and I. Cotton, "Automated four-point probe measurement of individual nanowires inside a scanning electron microscope," *IEEE Trans. Nanotechnol.*, vol. 10, no. 4, pp. 674–681, Jul. 2011.

[30] M. Rosenberger, M. J. Schaub, S. C. N. Töpfer, and G. Lin, "High efficiency strain measurements with small strain gauges using the time to digital converter principle," in *Proc. 6th Int. Conf. Meas.*, 2007, pp. 292–295.

[31] L. van Kouwen, A. Botman, and C. W. Hagen, "Focused electron-beam-induced deposition of 3 nm dots in a scanning electron microscope," *Nano Lett.*, vol. 9, no. 5, pp. 2149–2152, May 2009.


**Chao Zhou** received the B.S. degree (Hons.) in automation from Southeast University, Nanjing, China, in July 2003, and the Ph.D. degree in control theory and control engineering from the Institute of Automation, Chinese Academy of Sciences, Beijing, China, in 2008.

He is with the Key Laboratory of Complex Systems and Intelligent Science, Institute of Automation, Chinese Academy of Sciences, where he has been an Assistant Professor since July 2008 and Associate Professor since October 2011. His current research interests include the motion control of robot, the bio-inspired robotic fish, and embedded system of robot.

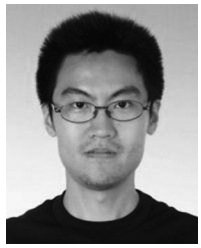

**Zheng Gong** received the B.S. degree in computer science from Xi'an Jiaotong University, Xi'an, China, in 2004, the M.S. degree in computer science from Zhejiang University, Hangzhou, China, in 2006, and the Ph.D. degree in mechanical engineering from the Tokyo Institute of Technology, Tokyo, Japan, in 2012.

From 2012 to 2014, he was a Postdoctoral Fellow with the University of Toronto, Toronto, ON, Canada. He is currently a Software Engineer at Aon Benfield, Toronto. His research interests include the image processing, computer vision, and robotics.

**Brandon K. Chen** received the Ph.D. degree in mechanical engineering from the University of Toronto, Toronto, ON, Canada, in 2013.

His research is in micro-nano robotic manipulation under SEM, with a focus on fabrication and control of MEMS-based manipulation tools, nanomaterials and nanostructures characterization, and single cell subnuclear surgery. He is currently leading the effort in the commercialization of precision instruments with support from Ontario Centres of Excellence and the Heffernan/Co-Steel Innovation Commercialization Fellowship.

**Zhiqiang Cao** received the B.S. and M.S. degrees from the Shandong University of Technology, Shandong, China, in 1996 and 1999, respectively, and the Ph.D. degree in control theory and control engineering from the Institute of Automation, Chinese Academy of Sciences, Beijing, China, in 2002.

He is currently an Associate Professor in the State Key Laboratory of Management and Control for Complex Systems, Institute of Automation, Chinese Academy of Sciences. His research interests include embedded vision and visual cognition, robot control and multirobot systems.

**Junzhi Yu** (SM'14) received the B.E. degree in safety engineering and the M.E. degree in precision instruments and mechanology from the North China Institute of Technology (currently North University of China), Taiyuan, China, in 1998 and 2001, respectively, and the Ph.D. degree in control theory and control engineering from the Institute of Automation, Chinese Academy of Sciences (IACAS), Beijing, China, in 2003.

He is currently a Professor in the State Key Laboratory of Management and Control for Complex Systems, IACAS. His research interests include biomimetic robots, intelligent control, and intelligent mechatronic systems.

**Changhai Ru** received B.S. and M.S. degrees from the Harbin University of Commerce, Harbin, China, in 1999 and 2002, respectively, and the Ph.D. degree from the Harbin Institute of Technology, Harbin, in 2005, all in mechanical engineering.

He is a Professor with the Research Center of Robotics and Micro System, Soochow University, Suzhou, China. His research areas include microrobotics and nanorobotic manipulation, nanopositioning technology, and automated instrumentation for biomedical applications.

**Min Tan** received the B.Sc. degree from Tsinghua University, Beijing, China, in 1986, and the Ph.D. degree from the Institute of Automation, Chinese Academy of Sciences (IACAS), Beijing, China, in 1990, both in control science and engineering.

He is currently a Professor with the State Key Laboratory of Management and Control for Complex Systems, IACAS. He has published more than 200 papers in journals, books, and conference proceedings. His research interests include robotics and intelligent control systems.

**Shaorong Xie** received the Ph.D. degree in mechanical engineering from Tianjin University, Tianjin, China, in 2001, and did her postdoctoral research at the University of Toronto.

She is a Professor in the School of Mechatronic Engineering and Automation, Shanghai University, Shanghai, China.

Dr. Xie's research project, "The intelligent control system of Unmanned Surface Vehicle," won the 2015 first-place Scientific Progress Award of Shanghai Municipality. Among her awards were the Excellent Subject Chief Scientist of Shanghai Municipality in 2012, Rising-Star of Science and Technology of Shanghai Municipality in 2012 and 2007.

**Yu Sun** (F'15) received the Ph.D. degree in mechanical engineering from the University of Minnesota, Minneapolis, MN, USA, in 2003 and did his postdoctoral research at ETH-Zürich.

He is a Professor in the Department of Mechanical and Industrial Engineering, with joint appointments in the Institute of Biomaterials and Biomedical Engineering and the Department of Electrical and Computer Engineering at the University of Toronto. He is currently a McLean Senior Faculty Fellow at the University of Toronto and the Canada Research Chair in Micro and Nano Engineering Systems. In 2012 and 2013, he directed the University of Toronto Nanofabrication Center.

Dr. Sun has served and serves on the editorial boards of several IEEE Transactions, *J. Micromechanics Microengineering*, *Scientific Reports*, and *Microsystems & Nanoengineering*. He was elected Fellow of American Society of Mechanical Engineers and Canadian Academy of Engineering for his work on micro-nano devices and robotic systems.